



## Ansae in NGC 253

J.A. Camperi<sup>1</sup>, H. Dottori<sup>4</sup>, G. Günthardt<sup>1</sup>, R.J. Díaz<sup>1,3</sup> & M.P. Agüero<sup>1,2</sup>

<sup>1</sup> Observatorio Astronómico de Córdoba, UNC, Argentina

<sup>2</sup> Consejo Nacional de Investigaciones Científicas y Técnicas, Argentina

<sup>3</sup> Gemini Observatory, EE.UU.

<sup>4</sup> Instituto de Física, Universidade Federal do Rio Grande do Sul, Brasil

Received: 09 February 2024 / Accepted: 29 June 2024

©The Authors 2024

**Resumen** / A partir de imágenes infrarrojas obtenidas con el instrumento Flamingos-2 del telescopio Gemini Sur en las bandas J, H y  $K_s$ , presentamos la detección de estructuras diferenciadas en los extremos de la barra de NGC 253 (conocidas como ansae). Estructuras de este tipo se observan en aproximadamente el uno por ciento de las galaxias, y las ansae de NGC 253 son las más cercanas detectadas a la fecha. Su cercanía, sumada a la alta resolución espacial de nuestras observaciones permitió caracterizarlas por primera vez como estructuras espacialmente resueltas. Utilizamos diagramas color-color (CCD) y color-magnitud (CMD) de los cúmulos de emisión infrarroja de las ansae y los comparamos con los de diversos subsistemas de la galaxia (núcleo, brazos, barra). Aplicamos modelos evolutivos para caracterizar y comparar las poblaciones de cúmulos predominantes en los diferentes subsistemas galácticos. Entre los diagramas color-color confeccionados se consideró uno que incluye el índice de color  $Q_d$  (asociado con la edad de los cúmulos), por lo que se dispone de un indicador para cuantificar la proporción de las poblaciones jóvenes en estos subsistemas. En las ansae de NGC 253 hay una notable separación de valores en el índice  $Q_d$  para la población noreste y la población suroeste de cúmulos y existe una mayor proporción de fuentes brillantes en la ansae suroeste. En términos de colores y población, las ansae se diferencian de la barra y por tanto deben ser de ahora en más consideradas como una componente adicional en la estructura de NGC 253.

**Abstract** / From infrared images obtained with the Flamingos-2 instrument of the Gemini South telescope in the J, H, and  $K_s$  bands, we present the detection of differentiated structures at the ends of the NGC 253's bar (known as ansae). Structures of this type are observed in approximately one percent of galaxies, and the ansae of NGC 253 are the closest ones detected to date. Its proximity, added to the high spatial resolution of our observations, allowed us to characterize them for the first time as structures spatially resolved. We use color-color diagrams (CCD) and color-magnitude diagrams (CMD) of the infrared emission clusters of the ansae and we compare them with those of various subsystems of the galaxy (core, arms, bar). We apply evolutionary models to characterize and compare predominant cluster populations in the different galactic subsystems. Among the color-color diagrams constructed was one that included the color index  $Q_d$ , which is associated with the age of the clusters. This provides an age indicator to quantify the proportion of young clusters in these subsystems. In the ansae of NGC 253 there is a notable separation of values in the  $Q_d$  index for the northeast population and the southwest population of clusters and there is a greater proportion of bright sources in the ansae southwest. In terms of colors and population, the ansae differ from the bar and therefore must be from now in more considered as an additional component in the structure of NGC 253.

**Keywords** / galaxies: starburst — galaxies: spiral — galaxies: photometry — galaxies: structure — galaxies: individual (NGC 253)

### 1. Introduction

The term ansae, in the context of the morphology of barred galaxies, makes reference to density enhancements at the ends of the bar (see the image of NGC 253 in Fig. 1), sometimes also referred to as “condensations” in older works (Danby, 1965), or symmetric density knots. A more scientific definition could be “a local maximum before the end of the bar along its main axis and absent on its minor axis” (Martinez-Valpuesta et al., 2007). It was first introduced, in the specific context of the study of starburst galaxies, by Buta et al. (1995). A close visual inspection of atlas images of the 600 closest galaxies in the southern hemisphere, shows that only 6 have visible ansae, with an average distance

of 23 Mpc. Only 14 % of the barred galaxies have some type of ansae (Martinez-Valpuesta et al., 2007). The presence of these structures in NGC 253 ( $d = 3.94 \pm 0.37$  Mpc, where  $1'' \sim 17$  pc; Karachentsev et al. 2003) enhance our understanding by allowing detailed study of the constituent star clusters, which are resolved through high spatial resolution ground-based observations. However, the ansae were not detected and studied before due to the high inclination of the galaxy, which causes significant intrinsic obscuration in optical wavelengths.

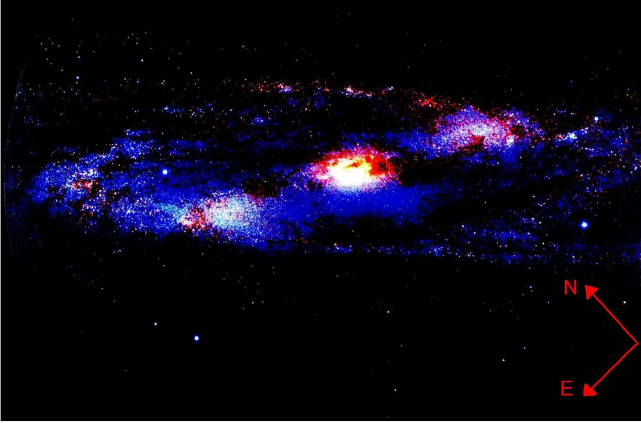


**Fig. 1.** Pseudocolor JHK<sub>s</sub> Flamingos-2 (Gemini South telescope, program GS-F2-MOSCOM-2016B) image of NGC 253 with a non-linear display scale to enhance the brightest structural components in the near-infrared, depicting the ansae at the tips of the bar. The red tones indicate the most obscured regions (highest K<sub>s</sub>/J ratio).

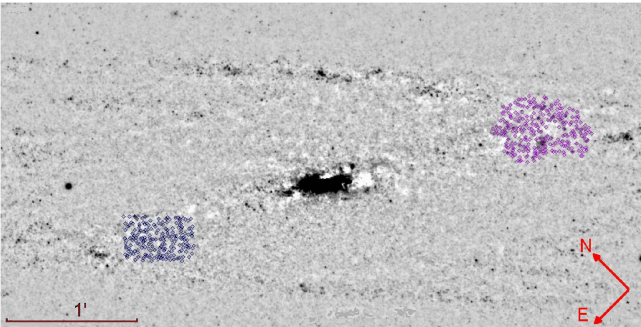


**Fig. 2.** Identification of luminous clusters in the northeast (blue, 192 sources) and southwest (purple, 249 sources) ansae in the residual K<sub>s</sub> band image.

## 2. Ansae in NGC 253

Many efforts have been devoted to the study of nuclear and circumnuclear star formation in galaxies, mainly interested in studying the feeding mechanisms of the super-massive black hole (e.g. Esquej et al., 2014; Agüero et al., 2016; Riffel et al., 2016). Since 2011 we have been studying the structure and dynamics of the central region of NGC 253 in order to shed light on the feeding mechanisms of the starburst and its possible relationship with the existence of a super-massive black hole outside the center of symmetry of the galaxy (Camperi et al., 2012, 2015). The presence of structures such as ansae, capable of modulating feeding mechanisms in several ways, cannot escape our attention.

## 3. Observations and data reduction

Direct images of NGC 253 with Flamingos-2 (Eikenberry et al., 2008; Diaz et al., 2013) have been obtained at Gemini South, in the J, H, and K<sub>s</sub> bands with an average spatial resolution of 0''.5. The images were reduced using THELI (Schirmer, 2013). Then we applied

a standard mask procedure with the IRAF \* package: the frames went through a process of filtering that consisted of the successive use of two IRAF subroutines (median and gauss) to produce highly smoothed frames taking into account the galaxy background. Then the smoothed frames were subtracted from the original ones to generate residues where the various infrared sources were much better evidenced.

To identify the clusters we used the SExtractor code (Bertin & Arnouts, 1996), a neural network-based algorithm, widely used by the community during the last 25 years. SExtractor made it possible to automatically detect the luminous sources on our infrared images and get their coordinates and photometry in a particularly simple and direct way (see Fig. 2). The photometric calibration and zero points were determined following the methodology outlined in Günthardt et al. (2015).

## 4. Color-magnitude diagrams

We have constructed a classic color-magnitude diagram (CMD) (J-K<sub>s</sub>) vs. M<sub>k</sub> (see Fig. 3), and we compared our observational data with the theoretical isochrones of Padova (Marigo et al., 2008) with the Initial Mass Function of Chabrier (Chabrier, 2003), a metallicity Z = 0.02, and running the simulation up to an age t ~ 14.8 × 10<sup>9</sup> yr (see Figs. 3 and 4). For control, we also used the Starburst 99 (SB99) code (Leitherer et al., 1999). In addition, we also constructed a reddening-free color-magnitude diagram using the Q<sub>d</sub> index (Israel et al., 1998; Witt et al., 1992) (see Fig. 4), following the approach outlined in Grosbøl & Dottori (2012). The Q<sub>d</sub> index characterizes reddening-corrected color under the assumption of well-mixed dust and stars, while another reddening-free index, Q<sub>s</sub>, can be formulated under the assumption of dust screening the stars (Indebetouw et al., 2005). We opted to analyze the distribution of clusters in the Q<sub>d</sub> vs. M<sub>k</sub> reddening-free diagram. This choice works well with the problem of extinction, as the majority of clusters that appeared scattered in the CMD are concentrated on the descending branch of the models in the Q<sub>d</sub> versus M<sub>k</sub> diagram (Fig. 4).

## 5. Color-color diagram

Figure 5 shows the (J-H) vs. (H-K<sub>s</sub>) diagram. The figure also shows the dereddening vector for two extreme models: 1- dust well mixed with the stars (black arrow), as can be seen in Witt et al. (1992) and Israel et al. (1998); 2- a screen model of the dust (pink arrow), as can be seen in Indebetouw et al. (2005).

It is worth mentioning that the Padova models do not take into account the ionized gas line emission, contrary to SB99 (Leitherer et al., 1999). This fact explains the differences between both models shown in Fig. 5.

\*IRAF is distributed by the National Optical Astronomy Observatories, which are operated by the Association of Universities for Research in Astronomy, Inc., under a cooperative agreement with the National Science Foundation.

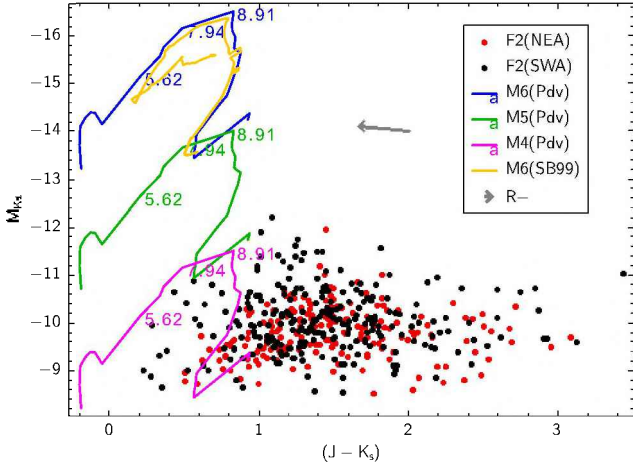


**Fig. 3.** Color-magnitude diagram for the index  $(J-K_s)$  of the ansae northeast (NEA; red dots) and southwest (SWA; black dots). The Padova curves (Pdv) for different masses ( $10^6 M_\odot$  in blue,  $10^5 M_\odot$  in green, and  $10^4 M_\odot$  in pink), along with the SB99 curve ( $10^6 M_\odot$  in ochre) are displayed. The numbers next to the lines are the elapsed simulation times in millions of years. It is added in this diagram R-, which represents the dereddening vector for this particular CMD.

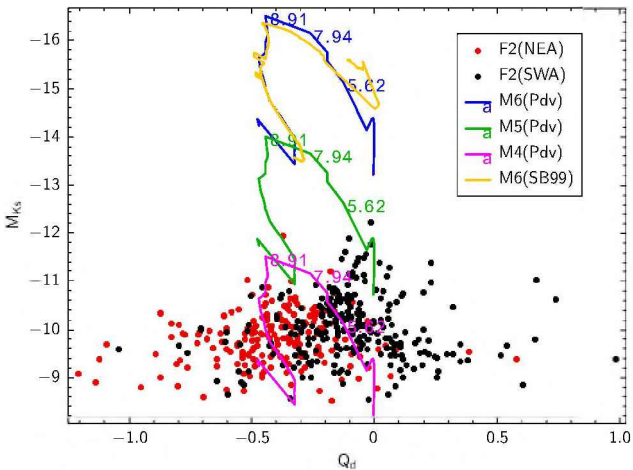


**Fig. 4.** Color-magnitude diagram for the index  $Q_d$  of the northeast (NEA; red dots) and southwest (SWA; black dots) ansae. Also shown for different masses are the Padova and SB99 curves (same symbology than in Fig. 3).

## 6. Analysis

We could detect the ansae of NGC 253 and its component clusters. This was achieved with the conjunction of an 8-meter class telescope (Gemini South Telescope) and a peripheric tool optimized for operating in the near infrared (Flamingos-2), with enough resolution. The use of standard masking techniques, plus neural-based algorithms, provided the quantitative results for comparing our data with evolutionary models. With this, we were capable of characterize the ansae as very young structures.

On the other hand, our data can be used for direct, simple statistical comparisons between the two ansae. From them, it is noticeable that there are statistical dif-

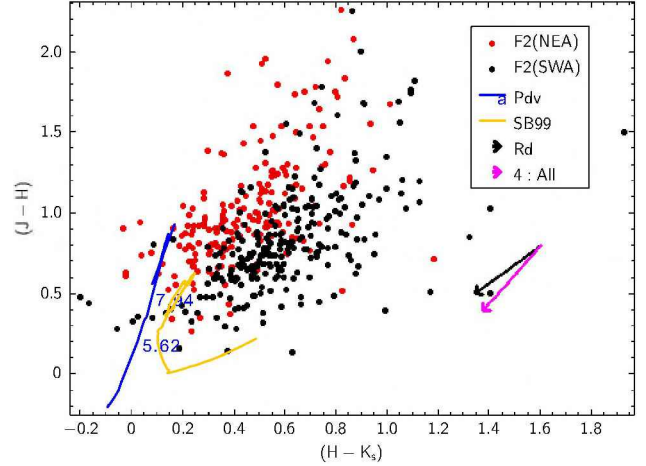


**Fig. 5.** Color-color diagram of the ansae northeast (NEA; red dots) and southwest (SWA; black dots). The Padova and SB99 curves are displayed, as well as the dereddening vectors (dust model - black arrow - and screen model - pink arrow). Same symbology than in Fig. 3.

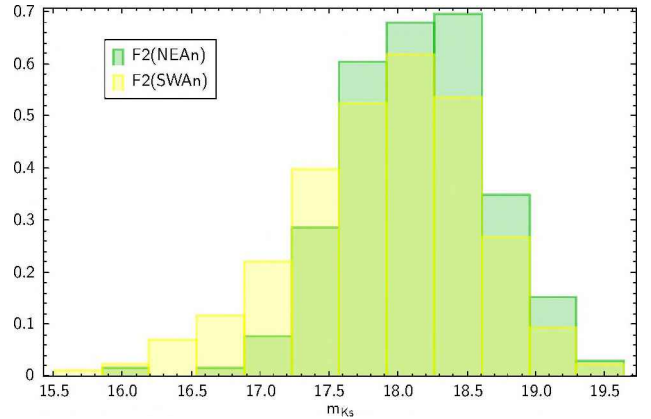


**Fig. 6.** Histogram of the ansae's apparent magnitudes in the  $K_s$  band. F2(NEAn) denotes the bars for the northeast ansae and F2(SWAn) denotes the bars for the southwest ansae.

ferences between the northeast and the southwest ansae. We can look at the histograms in the Fig. 6, Fig. 7 and Fig. 8. In Fig. 6 we see that the maximum number of clusters is found at  $m_{K_s} = 18.10 \pm 0.15$  mag for the northeast ansae and  $m_{K_s} = 17.9 \pm 0.15$  mag for the southwest. In the southwest structure, there are 9 sources brighter than  $m_{K_s} = 16.5 \pm 0.1$  mag, whereas in the northeast, there is only one. This proportion is much larger than the statistical relationship between both samples.

In Fig. 7 no differential reddening is observed on one side with respect to the other if we use the  $(J-K_s)$  color index. However, this index is susceptible to the effects of the presence of dust.

In the study conducted by Santos et al. (2013), it is proposed that the age distribution of clusters up to 100 Myr can be classified into two categories: clusters older and younger than 7 Myr, based on whether  $Q_d < 0.1$  or  $Q_d > 0.1$  respectively. As shown in Fig. 8, by

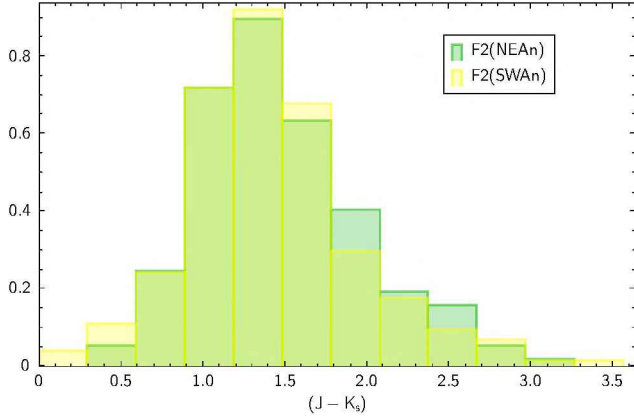


**Fig. 7.** Histogram of the ansae's  $(J-K_s)$  color index. The notations F2(NEAn) and F2(SWAn) have the same meaning as in Fig. 6.

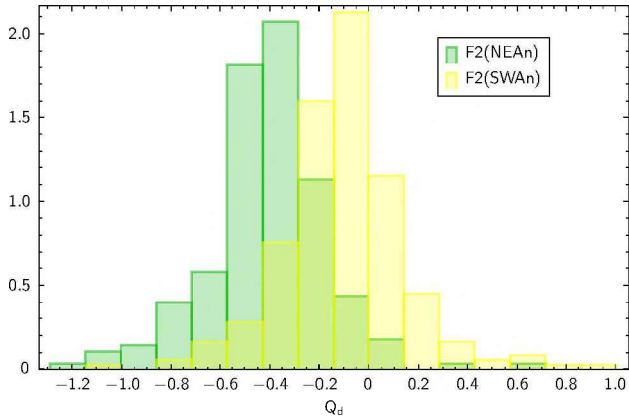


**Fig. 8.** Histogram of the ansae's  $Q_d$  color index. The notations F2(NEAn) and F2(SWAn) have the same meaning as in Fig. 6.

applying this criterion to our clusters, we observe that across all substructures, there is a higher proportion of young clusters in the southwest sector compared to the northeast.

This research is part of a broader study covering the entirety of NGC 253. For detailed information on the nuclear and circumnuclear regions of NGC 253, we refer the reader to Camperi et al. (2022).

## 7. Summary

The utilization of CMD and CCD diagrams, coupled with the simple statistical data, has enabled us to delin-

ate the northeast and southwest ansae as distinct structures, representing separate populations. This characterization will serve as the focal point for future investigations.

*Acknowledgements:* Based on observations obtained at the Gemini Observatory, which is operated by the Association of Universities for Research in Astronomy, Inc., under a cooperative agreement with the NSF on behalf of the Gemini partnership: the National Science Foundation (United States), the National Research Council (Canada), CONICYT (Chile), Ministerio de Ciencia, Tecnología e Innovación Productiva (Argentina), and Ministério da Ciência, Tecnologia e Inovação (Brazil).

## References

- Agüero M.P., Díaz R.J., Dottori H., 2016, *International Journal of Astronomy and Astrophysics*, 6, 219
- Bertin E., Arnouts S., 1996, *A&AS*, 117, 393
- Buta R., Purcell G.B., Crocker D.A., 1995, *AJ*, 110, 1588
- Camperi J.A., et al., 2012, *Boletín de la Asociación Argentina de Astronomía La Plata Argentina*, 55, 253
- Camperi J.A., et al., 2015, *Boletín de la Asociación Argentina de Astronomía La Plata Argentina*, 57, 28
- Camperi J.A., et al., 2022, *Boletín de la Asociación Argentina de Astronomía La Plata Argentina*, 63, 232
- Chabrier G., 2003, *PASP*, 115, 763
- Danby J.M.A., 1965, *AJ*, 70, 501
- Díaz R.J., et al., 2013, *Boletín de la Asociación Argentina de Astronomía La Plata Argentina*, 56, 457
- Eikenberry S., et al., 2008, I.S. McLean, M.M. Casali (Eds.), *Ground-based and Airborne Instrumentation for Astronomy II, Society of Photo-Optical Instrumentation Engineers (SPIE) Conference Series*, vol. 7014, 70140V
- Esquej P., et al., 2014, *ApJ*, 780, 86
- Grosbøl P., Dottori H., 2012, *A&A*, 542, A39
- Günthardt G.I., et al., 2015, *AJ*, 150, 139
- Indebetouw R., et al., 2005, *ApJ*, 619, 931
- Israel F.P., et al., 1998, *A&A*, 336, 433
- Karachentsev I.D., et al., 2003, *A&A*, 404, 93
- Leitherer C., et al., 1999, *ApJS*, 123, 3
- Marigo P., et al., 2008, *A&A*, 482, 883
- Martínez-Valpuesta I., Knapen J.H., Buta R., 2007, *AJ*, 134, 1863
- Riffel R.A., et al., 2016, *MNRAS*, 461, 4192
- Santos J.F.C., Dottori H., Grosbøl P., 2013, *A&A*, 553, A74
- Schirmer M., 2013, *ApJS*, 209, 21
- Witt A.N., Thronson Harley A. J., Capuano John M. J., 1992, *ApJ*, 393, 611